PERGAMON

International Journal of Solids and Structures 39 (2002) 5585–5614

INTERNATIONAL JOURNAL OF SOLIDS and STRUCTURES

www.elsevier.com/locate/ijsolstr

Wave propagation in nonlinear and hysteretic media—a numerical study

T. Meurer [a,*], J. Qu [b], L.J. Jacobs [c]

[a] *Institute of System Dynamics and Control Engineering, University of Stuttgart, Pfaffenwaldring 9, 70569 Stuttgart, Germany*
[b] *GWW School of Mechanical Engineering, Georgia Institute of Technology, Atlanta, GA 30332-0405, USA*
[c] *School of Civil and Environmental Engineering, Georgia Institute of Technology, Atlanta, GA 30332-0355, USA*

Received 15 January 2002; received in revised form 3 April 2002

Abstract

This paper considers the problem of one dimensional wave propagation in nonlinear, hysteretic media. The constitutive law in the media is prescribed by an integral relationship based on the Duhem model of hysteresis. It is found that the well known nonlinear elastic stress–strain relationship is a special case of this integral relationship. It is also shown that the stress–strain relationship from the McCall and Guyer model of hyesteretic materials can also be derived from this integral stress–strain relationship. The first part of this paper focuses on a material with a quadratic stress–strain relationship, where the initial value problem is formulated into a system of conservation laws. Analytical solutions to the Riemann problem are obtained by solving the corresponding eigenvalue problem and serve as reference for the verification and illustration of the accuracy obtained using the applied numerical scheme proposed by Kurganov and Tadmor. The second part of this research is devoted to wave propagation in hysteretic media. Several types of initial excitations are presented in order to determine special characteristics of the wave propagation due to material nonlinearity and hysteresis. The results of this paper demonstrate the accuracy and the robustness of this numerical scheme to analyze wave propagation in nonlinear materials.

Keywords: Wave propagation; High-resolution scheme; Conservation law; Nonlinear media; Hysteretic media; Integro-differential equations

1. Introduction

Ultrasonic nondestructive evaluation has evolved into an interdisciplinary area of intensive research with a broad variety of applications from noninvasive medical diagnosis to the development of new materials and their characterization. Nondestructive evaluation includes the development of new measurement technologies to make quantitative assessment of micro- and macro-structural properties as well as the

* Corresponding author. Tel.: +49-711-685-6568.
E-mail addresses: thomas.meurer@isr.uni-stuttgart.de (T. Meurer), jianmin.qu@me.gatech.edu (J. Qu), laurence.jacobs@ce.gatech.edu (L.J. Jacobs).

0020-7683/02/$ - see front matter
PII: S0020-7683(02)00366-9

corresponding analysis techniques to fully understand and interpret the obtained results. Since measurement, analysis, and the development of theoretical foundations interact, the study of wave propagation in materials and hence their characterization has become a challenging discipline.

Traditional ultrasonic techniques rely on wave propagation in linear elastic media. Such techniques are effective in detecting flaws in materials and structures. However, techniques based on the propagation of nonlinear waves are often more effective for evaluating and characterizing mechanical/physical properties pertaining to reliability, durability and remaining life of materials and structure components (e.g., Liu et al., 2000). These properties may include fatigue strength, dislocation density, interfacial bond strength, curing state of polymers, chemical and physical aging, etc. In addition, some materials are inherently nonlinear and hysteretic, such as rocks (e.g., McCall, 1994; McCall and Guyer, 1994).

The objective of this paper is to present a numerical study of propagating pulsed and harmonic waves in nonlinear, history-dependent media—hysteretic media—using a high-resolution numerical scheme. This study focuses on longitudinal, one-dimensional wave propagation.

The observation of nonlinear effects in laboratory experiments originating in either damaged materials or naturally nonlinear materials such as rock or sandstone yields a basis for the development of an underlying theory of propagating waves. Since the governing equations are nonlinear, hyperbolic partial differential equations, closed form solutions exist only in a few special cases. The application of perturbation methods yields asymptotic solutions, with the disadvantages of a rather demanding and complicated analysis and an often nonobvious and indeterminable interval of solution validity. On the other hand, there are many numerical solution algorithms that have been developed and applied successfully in computational fluid dynamics (CFD) in order to approximate the solution of nonlinear wave propagation problems. These methods can be extended to multidimensional problems and inhomogeneous nonlinear problems.

Some basic mathematical concepts are required in order to understand the development of any approximations associated with the numerical solution, as well as the evolving nonlinear effects, such as shock and rarefaction waves. These mathematical preliminaries are introduced based on the conservation property of the governing one-dimensional wave equation. Hence hyperbolic systems of conservation laws are studied in theory and numerical experiments. The development of numerical solution algorithms is based on the specific mathematical structure of the governing equations. There are two basic approaches, upwind and central schemes, that originate from CFD. In this paper, a second-order, high-resolution central scheme proposed by Kurganov and Tadmor (2000) is used—see Appendix B for a brief summary of the numerical algorithm.

There has been extensive work in the published literature on nonlinear wave propagation, see Kolsky (1963), Bland (1969), Debnath (1997), Drumheller (1998), Whitham (1999), Hamilton and Blackstock (1998) and Naugolnykh and Ostrovsky (1998) for an introduction and review of suitable techniques. The review article by Norris (1998) provides a comprehensive review of nonlinear wave propagation in solids.

Recently, significant progress has been made towards a better understanding of wave propagation in heterogeneous materials such as rocks by McCall and Guyer (1994), McCall and Guyer (1996), Guyer and McCall (1995), Van Den Abeele et al. (2000a); Van Den Abeele et al. (2000b) and Gusev (2000). In their work, the Preisach–Mayergoyz (P–M) description of hysteretic systems was utilized to develop a constitutive model at the mesoscopic level for wave propagation in heterogeneous geomaterials like rocks, sandstones, concrete, and soil. Using the Green's function method in conjunction with a perturbation technique, they were able to obtain quasi-analytical solutions for the nonlinear wave propagation in hysteretic media described by the P–M model of hysteresis.

This paper focuses on hysteresis of a different type. In this description of hysteresis, the constitutive equation relating stress and strain is given by an integral equation. This model was first proposed by Hodgdon in Hodgdon (1988a) and Hodgdon (1988b) for the case of electromagnetics. It provides active

hysteretic behavior, while allowing for the development of residual strains corresponding to plastic deformation as well as residual stresses. Furthermore, this paper shows that the stress–strain relationship based on the Hodgdon model of hysteresis can be reduced to that of the P–M model of hysteresis by properly selecting the functions in the Hodgdon model.

The paper is arranged as follows. Hodgdon's description of hysteresis is briefly outlined in Section 2. It is also shown there how the P–M model can be derived from the Hodgdon model. Section 3 focuses on nonlinear elastic material without hysteresis and Section 4 is for materials with both nonlinearity and hysteresis. Some concluding remarks are presented in Section 5.

2. Nonlinear constitutive laws

For materials with distributed damage (micro-cracks, micro-voids), and for materials under plastic deformation, linear elastic Hooke's law is usually inadequate to describe their nonlinear, inelastic behavior. Various constitutive laws have been proposed. This paper studies the class of materials whose behavior can be described by the following stress–strain relationship,

$$\frac{\partial\sigma(\epsilon,\dot{\epsilon})}{\partial\epsilon} = g(\epsilon) - \alpha s[\sigma(\epsilon_0) - f(\epsilon_0)]e^{\alpha s(\epsilon_0-\epsilon)} - \alpha s\int_{\epsilon_0}^{\epsilon}\left[g(\tau) - \frac{df(\tau)}{d\tau}\right]e^{\alpha s(\tau-\epsilon)}\,d\tau, \tag{1}$$

or

$$\sigma(\epsilon,\dot{\epsilon}) = f(\epsilon) + [\sigma(\epsilon_0) - f(\epsilon_0)]e^{\alpha s(\epsilon_0-\epsilon)} + \int_{\epsilon_0}^{\epsilon}\left[g(\tau) - \frac{df(\tau)}{d\tau}\right]e^{\alpha s(\tau-\epsilon)}\,d\tau, \tag{2}$$

where ϵ_0 is the initial strain, $s = \mathrm{sign}(\dot{\epsilon})$, α is a constant, and $f(\epsilon)$ and $g(\epsilon)$ are functions to be determined experimentally for a given material. In the above equations and in the following sections, a dot overhead indicates derivative with respect to time. Macki et al. (1993) and Mayergoyz (1991) show that with proper selection of α, $f(\epsilon)$ and $g(\epsilon)$, the constitutive law described in (1) or (2) can be used to describe a wide range of material behavior.

This section shows how (1) or (2) can be reduced to the traditional nonlinear elastic stress–strain law, and how it can be reduced to the P–M hysteretic model. To this end, consider a special case of (1) or (2), namely, no initial stress and strain. In this case,

$$\frac{\partial\sigma(\epsilon,\dot{\epsilon})}{\partial\epsilon} = g(\epsilon) + \alpha s f(0)e^{-\alpha s\epsilon} - \alpha s\int_{0}^{\epsilon}\left[g(\tau) - \frac{df(\tau)}{d\tau}\right]e^{\alpha s(\tau-\epsilon)}\,d\tau, \tag{3}$$

by setting $\alpha = 0$ and

$$g(\epsilon) = E(1 - \gamma\epsilon - \delta\epsilon^2 - \cdots), \tag{4}$$

one can reduce the stress–strain relationship of (3) to the well-known nonlinear elastic constitutive law,

$$\frac{\partial\sigma(\epsilon,\dot{\epsilon})}{\partial\epsilon} = E(1 - \gamma\epsilon - \delta\epsilon^2 - \cdots), \tag{5}$$

where E is the (second order) elastic (Young's) modulus, $E\gamma$ is called the third order elastic constant, and so on. Eq. (5) was derived by Landau and Lifshitz (1959) by expanding the strain energy density function for hyper-elastic materials.

Eq. (5) does not show any hysteresis in the stress–strain relationship. The hysteretic behavior is accounted for by using a nonzero α. Therefore, call α the hysteresis parameter. By substituting

$$\frac{\mathrm{d}f(\epsilon)}{\mathrm{d}\epsilon} = g(\epsilon) - E(1 + \alpha\Delta\epsilon), \quad f(0) = -\frac{E\Delta\epsilon}{s} \tag{6}$$

into (3), one obtains

$$\frac{\partial\sigma(\epsilon,\dot{\epsilon})}{\partial\epsilon} = g(\epsilon) - E(1 + \alpha\Delta\epsilon) + E\mathrm{e}^{-\alpha s\epsilon}. \tag{7}$$

For small values of α,

$$\mathrm{e}^{\pm\alpha s\epsilon} \approx 1 \pm \alpha s\epsilon. \tag{8}$$

Equation (7) together with (4) reduces to

$$\frac{\partial\sigma(\epsilon,\dot{\epsilon})}{\partial\epsilon} = E[1 - \gamma\epsilon - \delta\epsilon^2 - \alpha(\Delta\epsilon + s\epsilon)]. \tag{9}$$

This is identical to the stress–strain relationship derived in McCall and Guyer (1994); Guyer and McCall (1995) and Van Den Abeele et al. (2000a,b) based on the P–M model of hysteresis.

This demonstrates that the stress–strain relationship given by (1) or (2) is rather general and inclusive. By properly selecting the hysteresis parameter α and the functions $f(\epsilon)$ and $g(\epsilon)$, (1) or (2) can be used to describe a wide range of nonlinear elastic as well as hysteretic behavior. The stress–strain relationship (19), derived from the P–M model of hysteresis is a special case of (1) or (2) when only the leading order effect of α is taken into consideration.

Now, consider a one-dimensional problem of wave propagation through a nonlinear medium. For small strain deformation, the equation of motion can be written as (Achenbach, 1999)

$$\frac{1}{\rho}\frac{\partial\sigma}{\partial x} = \frac{\partial^2 u}{\partial t^2}, \tag{10}$$

where $u(x,t)$ is the displacement in the x-direction, ρ is the mass density, and $\sigma(x,t)$ is the normal stress in the x-direction. For the small strain deformation considered here, the normal strain in the x-direction, $\epsilon(x,t)$, is defined as

$$\epsilon = \frac{\partial u}{\partial x}. \tag{11}$$

Next, assume that the nonlinear constitutive relationship of the medium is described by

$$\sigma = \sigma(\epsilon,\dot{\epsilon}). \tag{12}$$

Substitution of (12) into (10) yields

$$\frac{1}{c^2}\frac{\partial^2 u}{\partial t^2} - \frac{\partial^2 u}{\partial x^2} = \left[\frac{1}{E}\frac{\partial\sigma}{\partial\epsilon} - 1\right]\frac{\partial^2 u}{\partial x^2}, \tag{13}$$

where E is the elastic Young's modulus and $c = \sqrt{E/\rho}$ can be considered as the phase velocity. Once $\sigma(\epsilon,\dot{\epsilon})$ is specified as a function of ϵ and $\dot{\epsilon}$, this nonlinear equation can be solved either numerically or asymptotically.

For convenience, define the state vector

$$\mathbf{v}(x,t) = \begin{bmatrix} v_1(x,t) \\ v_2(x,t) \end{bmatrix} = \begin{bmatrix} \dfrac{\partial u}{\partial t} \\ \dfrac{\partial u}{\partial x} \end{bmatrix}, \tag{14}$$

and the flux vector

$$\mathbf{f}(x,t) = \begin{bmatrix} \dfrac{-\sigma(v_2)}{\rho} \\ -v_1 \end{bmatrix} = \begin{bmatrix} \dfrac{-\sigma(\epsilon)}{\rho} \\ -\dfrac{\partial u}{\partial t} \end{bmatrix}. \tag{15}$$

Then, (10) can be written as

$$\frac{\partial \mathbf{v}}{\partial t} + \frac{\partial \mathbf{f}}{\partial x} = \mathbf{0}. \tag{16}$$

This so called conservation formulation is used in the remainder of this paper for analytical studies as well as numerical solution approximations.

3. Wave propagation in nonlinear elastic media

This section considers the case of a nonlinear material defined by the first two terms of (5),

$$\frac{\partial \sigma(\epsilon, \dot{\epsilon})}{\partial \epsilon} = E(1 - \gamma\epsilon), \tag{17}$$

or

$$\sigma = E(\epsilon - 0.5\gamma\epsilon^2). \tag{18}$$

Clearly, when $\gamma = 0$, the material is linear elastic. The parameter γ indicates the amount of material nonlinearity. As discussed in Gol'dberg (1961), for very weak material nonlinearity, one can show that the parameter γ defined here is identical to the acoustic nonlinear parameter (Cantrell and Yost, 1990). The acoustic nonlinear parameter arises in metals due to lattice anharmonicity which is usually very small in comparison to the elastic deformation of the metals. In contrast, this study focuses on strong nonlinear effects, such as those found in rubber-like materials, granular materials, and certain polymer materials. In these cases, the parameter γ is no longer the acoustic nonlinear parameter as traditionally defined.

Fig. 1 shows several stress–strain curves for $\gamma = 10000$, $\gamma = 5000$, and $\gamma = 2500$, respectively. Note that the constitutive equation given by (18) dictates that the material behaves differently in tension and

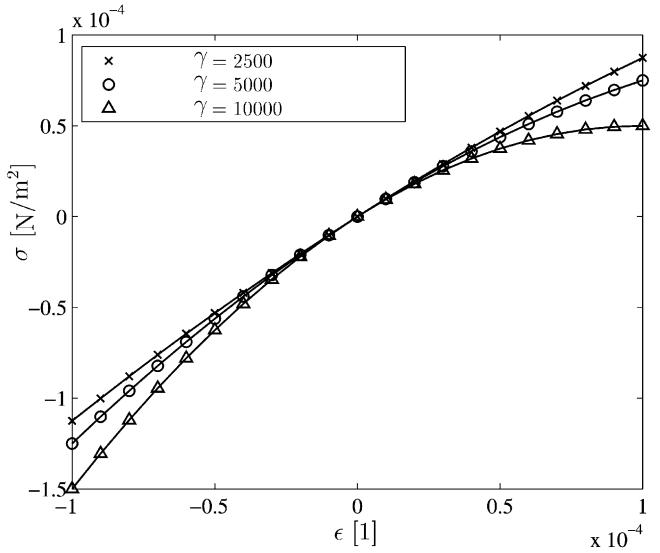

Fig. 1. Stress–strain curves for different values of γ.

compression, although the difference is only to the second order. In the literature, such material behavior is sometimes referred to as pseudo elastic. To model materials with identical nonlinear tensile and compressive behavior, only the quadratic terms in (5) should be used.

Substitution of (18) into (13) yields

$$\frac{\partial^2 u}{\partial t^2} = c^2\left(1 - \gamma\frac{\partial u}{\partial x}\right)\frac{\partial^2 u}{\partial x^2}. \tag{19}$$

This is the same equation derived by Gol'dberg (1961) based on the first principles of classical elasticity. Analytical solutions to (19) are only available for some special cases and hence numerical methods have to be applied to study the solution behavior. All further evaluations are based on the conservation law formulation introduced above. This paper follows a central scheme approach developed by Kurganov and Tadmor (2000) which can be applied to nonlinear conservation laws and convection–diffusion equations. It will be seen in the following sections that this numerical method provides a robust tool to handle severe discontinuities while providing excellent resolution of any nonlinear effect. The accuracy of this method is established by comparing the numerical solution with the analytical solution for the Riemann problem discussed in Section 3.2 and the Appendix A. Note that a brief summary of the numerical algorithm of Kurganov and Tadmor (2000) is presented in Appendix B.

3.1. Transformation into conservation form

In context of the conservation law formulation (16), Eq. (19) can be reformulated as

$$\frac{\partial}{\partial t}\begin{bmatrix} v_1 \\ v_2 \end{bmatrix} + \frac{\partial}{\partial x}\begin{bmatrix} -c^2 v_2\left(1 - \frac{\gamma}{2}v_2\right) \\ -v_1 \end{bmatrix} = 0, \tag{20}$$

with phase velocity $c = \sqrt{E/\rho}$. Consider Godlewski and Raviart (1996), Taylor (1996), Thomas (1995), and Thomas (1999) for general analysis of hyperbolic systems of conservation laws and the terminology used in the following. The eigenvalues of the Jacobian of the flux vector of system (20)

$$v_{1,2} = \mp c\sqrt{1 - \gamma v_2} \tag{21}$$

are real and distinct for $v_2 < 1/\gamma$. Hence system (20) is strictly hyperbolic under this condition. Furthermore, consider the corresponding eigenvectors

$$\mathbf{r}_{1,2}(v_2) = \begin{bmatrix} \pm c\sqrt{1 - \gamma v_2} \\ 1 \end{bmatrix}. \tag{22}$$

Both characteristic fields are genuinely nonlinear for $\gamma \neq 0$ (which will be assumed in what follows) since

$$\operatorname{grad} v_{1,2} \cdot \mathbf{r}_{1,2} = \frac{c\gamma}{2\sqrt{1 - \gamma v_2}} \neq 0 \tag{23}$$

holds. These properties of the system under consideration are exploited for the further analytical and numerical studies in the oncoming sections.

3.2. Discontinuous initial conditions—the Riemann problem

The specification of discontinuous initial conditions

$$\mathbf{v}(x, t = 0) = \begin{cases} \mathbf{v}_{\mathrm{L}} & \text{for } x < 0 \\ \mathbf{v}_{\mathrm{R}} & \text{for } x > 0, \end{cases} \tag{24}$$

for the hyperbolic two-system of conservation laws (20) serves two purposes. First, it will be used in this research to validate the numerical code for solving other types of initial conditions and the hysteresis

problem later in this paper. Second, the analysis below illustrates the evolving nonlinear dynamic effects, i.e. the development of shock and rarefaction waves. Note that the following comments and analytical considerations only hold for convex systems, i.e. strictly hyperbolic systems whose characteristic fields are either genuinely nonlinear or linearly degenerate (Godlewski and Raviart, 1996). Consult Wendroff (1972a,b) for the more general treatment of nonconvex systems. A closed form weak solution of the Riemann problem (20), (24) is derived in Meurer (2000), satisfying the Lax entropy condition. These results are summarized in Appedix A. In order to illustrate the solution behavior, consider the case of a one-shock followed by a two-rarefaction wave. Following Meurer (2000), the solution is hence governed at time $t = \tilde{t}$ by

$$\mathbf{v}(x,t_0) = \begin{cases} \mathbf{v}_{\mathrm{L}} & \text{for } x < s^{(1)}\tilde{t}, \\ \bar{\mathbf{v}} & \text{for } s^{(1)}\tilde{t} < x \leqslant v_2(\bar{\mathbf{v}})\tilde{t}, \\ \mathbf{w}^{(2)}(\xi = x/\tilde{t}) & \text{for } v_2(\bar{\mathbf{v}})\tilde{t} < x \leqslant v_2(\bar{\mathbf{v}}_{\mathrm{R}})\tilde{t}, \\ \mathbf{v}_{\mathrm{R}} & \text{for } x > v_2(\bar{\mathbf{v}}_{\mathrm{R}})\tilde{t}, \end{cases} \tag{25}$$

where $s^{(1)}$ denotes the one-shock speed given by (A.14), $\mathbf{w}^{(2)}(\xi = x/\tilde{t})$ the propagating two-rarefaction wave (A.11), and $\bar{\mathbf{v}}$ the evolving intermediate state connecting $\mathbf{v}_{\mathrm{L}}$ and $\mathbf{v}_{\mathrm{R}}$ in state-space (v_1, v_2).

The above analysis provides insight into the solution dynamics, in the sense that the left and right propagating states can only be connected by a one-wave followed by a two-wave. Furthermore, the evolving shock wave does not propagate along any characteristic line (21). From a numerical point of view, the tracking and resolution of a propagating shock wave is a rather challenging topic. Results obtained by a high-resolution central scheme approach developed by Kurganov and Tadmor (2000) are studied and compared with the analytical solution based on the results in Appendix A. Therefore consider the following discontinuous initial data

$$\mathbf{v}(x, t = 0) = \begin{cases} [0.1, -0.5]^{\mathrm{T}} & \text{for } x < 0, \\ [0.2, -1.0]^{\mathrm{T}} & \text{for } x > 0, \end{cases} \tag{26}$$

that describes the evolution of a one-shock (propagating to the left, i.e. $x < 0$) followed by two-rarefaction wave (propagating to the right, i.e. $x > 0$). The nonlinear parameter γ is set equal to 10 000, the phase velocity is set to unity. The numerical solution algorithm is initialized by $\Delta t = 10^{-6}$ s for the temporal step and by $\Delta x = 10^{-3}$ m for the spatial step in order to satisfy the Courant–Friedrichs–Lewy (CFL) (Thomas, 1999) condition of the particular problem. The numerical solution obtained by the high-resolution scheme of Kurganov and Tadmor (2000) as well as the analytical solution are depicted in Fig. 2 for the strain and in Fig. 3 for the particle velocity. This example establishes the accuracy and outstanding resolution capabilities of the proposed numerical scheme. It will be used in the following to solve other initial value problems (single and double wavenumber harmonic excitation) for both the quadratic constitutive equation and the hysteretic stress–strain relation.

3.3. Single-wavenumber harmonic excitation

Considering the results obtained for the Riemann problem in the previous section, nonlinear dynamic effects are expected to appear for the case of harmonic or sinusoidal initial conditions. In order to gain some insight into the solution dynamics, perturbation methods allow the analysis of the asymptotic behavior of this nonlinear system subjected to harmonic excitation—see Liu et al. (2000) and the references therein. These results indicate the appearance of higher order harmonics, i.e. integer multiples of the applied excitation frequencies or wavenumbers, respectively. In other words, after propagating through a nonlinear medium, an *originally* single wavenumber wave may contain wavenumber components other than the fundamental wavenumber. These results have been confirmed by experimental studies (Liu et al., 2000). If

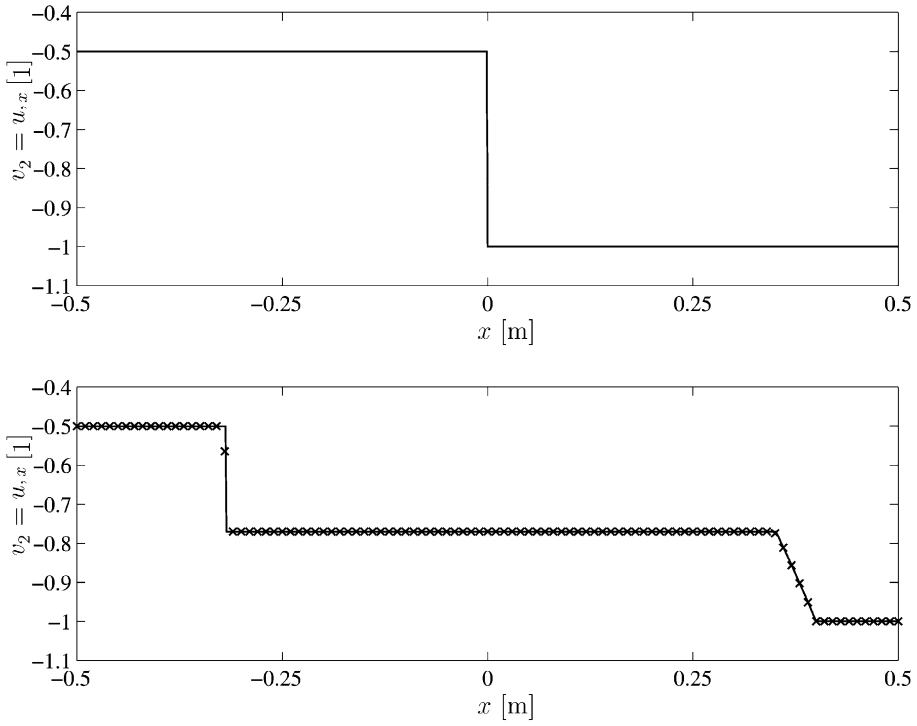

Fig. 2. Solution to the Riemann problem-strain. Top: initial data given by Equation (26). Bottom: Numerical solution (x) and exact solution (bold) at $t = 4.0 \times 10^{-3}$ s.

the nonlinearity of a particular medium is small, the perturbation approach yields sufficiently accurate results. If this is not the case (the nonlinearity is large) the asymptotic analysis must be extended to higher order terms in the solution ansatz and the algebra becomes rather complex. As a result, it is advisable to use numerical methods in order to obtain a sufficiently accurate solution, as well as a deeper understanding of the underlying nonlinear dynamics.

In this section, the governing equation (20) is solved under the initial excitation of a sinusoidal strain distribution over a finite length,

$$u_{,x}(x, t = 0) = \begin{cases} A \sin kx, & -150\Delta x \leqslant x \leqslant 150\Delta x, \\ 0, & \text{otherwise}, \end{cases} \tag{27}$$

$$u_{,t}(x, t = 0) = 0 \tag{28}$$

where, A denotes the amplitude and k determines the fundamental wavenumber. The numerical solution is carried out for $c = 70.71$ m/s, $\gamma = 10^4$, $A = 9.8 \times 10^{-5}$, and $k = 2.5 \times 10^5$ m^{-1}. The corresponding initial strain distribution is shown in Fig. 4. The numerical solution algorithm is initialized by $\Delta t = 10^{-10}$ s and $\Delta x = 10^{-7}$ m in order to satisfy the particular CFL-condition. These results illustrate that the initial sinusoidal strain distribution gradually evolves into a sawtooth profile, see Fig. 5 for the solution after 4000 time steps, i.e. $t = 4.0 \times 10^{-7}$ s. This is due to the fact that particles with higher strain propagate with slower speed than particles with lower strain. The wave profiles are distorted backward. This will eventually form shock waves behind each wave profile. The particle velocity distribution as shown in Fig. 6 at time $t = 4.0 \times 10^{-7}$ s also exhibits similar trends.

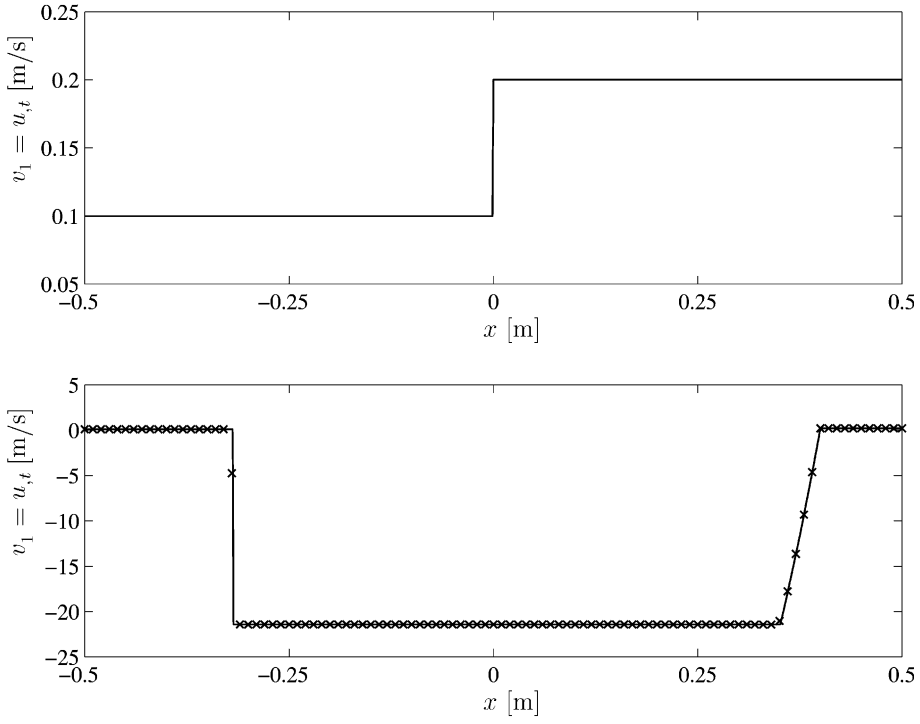

Fig. 3. Solution to the Riemann problem-particle velocity. Top: initial data given by Eq. (26). Bottom: Numerical solution (x) and exact solution (bold) at $t = 4.0 \times 10^{-3}$ s.

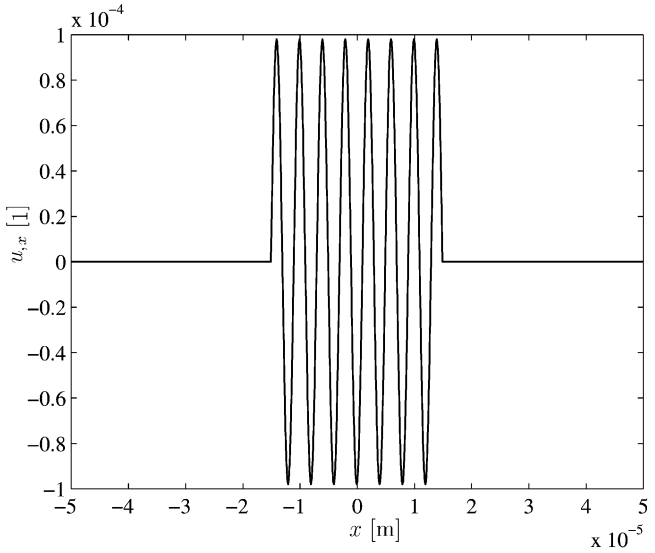

Fig. 4. Initial strain distribution given by Eq. (27).

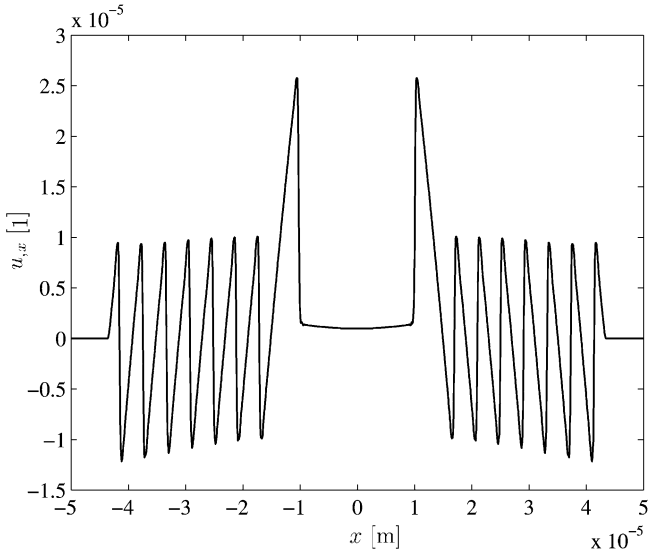

Fig. 5. Numerical solution for the strain wave at $t = 4.0 \times 10^{-7}$ s vs. x.

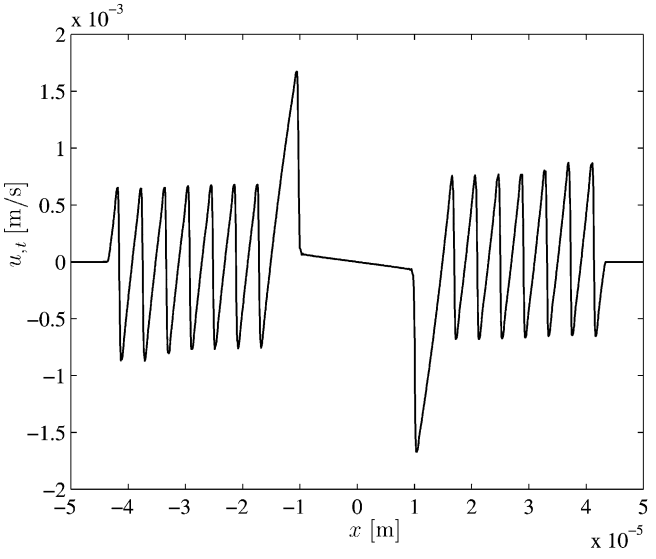

Fig. 6. Numerical solution for the particle velocity at $t = 4.0 \times 10^{-7}$ s vs. x.

An explanation for the development of a sawtooth profile can be given following Courant and Friedrichs (1976). Consider the characteristic shift rate (given by the eigenvalues (21) of the Jacobian of the flux vector)

$$| v_{1,2} | = c\sqrt{1 - \gamma v_2} = c\sqrt{1 - \gamma \frac{\partial u}{\partial x}}, \tag{29}$$

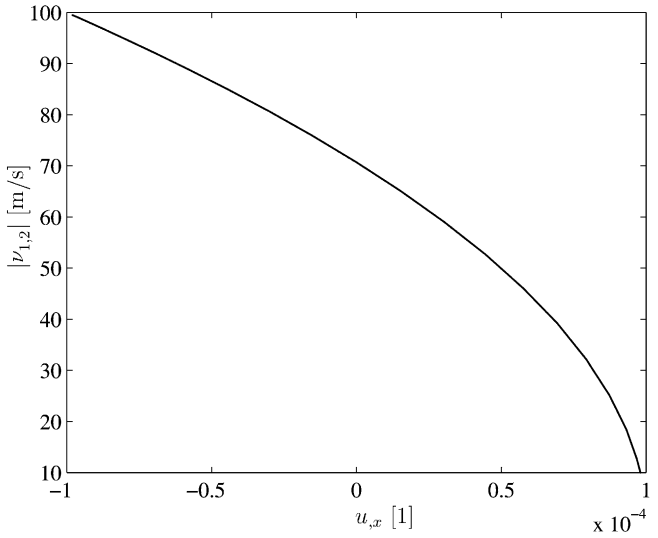

Fig. 7. Characteristic shift rate $|v_{1,2}|$ given by Eq. (29).

which is depicted in Fig. 7. While in tension, particles with higher strain values tend to propagate more slowly than those with lower strain values. Therefore, the front of the wave profile becomes more slanted while the back of the wave profile becomes more vertical. However, the situation in compression is different. According to (29), particles with higher compressive strain values propagate with higher speed than those with lower compressive strains. Therefore, for a compressive strain wave, the front of the wave profile will become more vertical as it propagates, while the back of the profile becomes more slanted. The combination of these two situations explains the evolution of the wave profiles shown in Figs. 5 and 6.

Fig. 8 shows the particle velocities at two locations, $x = -150\Delta x$ and $x = -250\Delta x$, as functions of time. Distortion of the wave profiles also generates higher order harmonics in the signal over space, at a fixed time, as well as in the signal over time at a fixed spatial position. Fig. 9 shows the fast Fourier transform (FFT) of the particle velocity ($v_1 = u_{,t}$), depicted in Fig. 6, with respect to the spatial variable x at a fixed time ($t = 4.0 \times 10^{-7}$ s)

$$\hat{v}_{1,2}(k,t) = \int_{-\infty}^{\infty} v_{1,2}(x,t)\exp(-2\pi \mathrm{i} k x)\,\mathrm{d}x. \tag{30}$$

The temporal FFT is defined as

$$\hat{v}_{1,2}(x,\omega) = \int_{0}^{\infty} v_{1,2}(x,t)\exp(-2\pi \mathrm{i}\omega t)\,\mathrm{d}t. \tag{31}$$

The result for a material particle at $x = -150\Delta x$ is shown in Fig. 10. These Figures show that for the material under consideration, even the fourth or the fifth order harmonics are clearly visible. The second order harmonics have also been obtained through a perturbation analysis, see for example, Liu et al. (2000). However, a rather complex and demanding perturbation analysis must be employed in order to obtain the third and fourth or higher order harmonics.

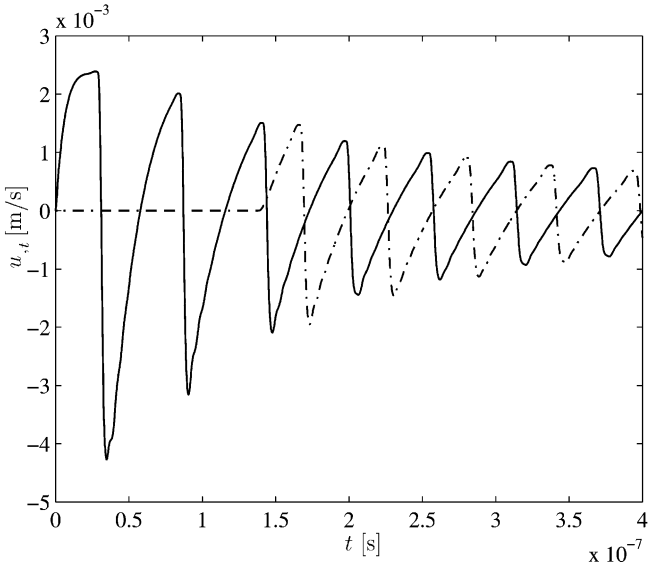

Fig. 8. Numerical solution for the particle velocity at $x = -150\Delta x$ (bold) and $x = -250\Delta x$ (dash-dot) over time t.

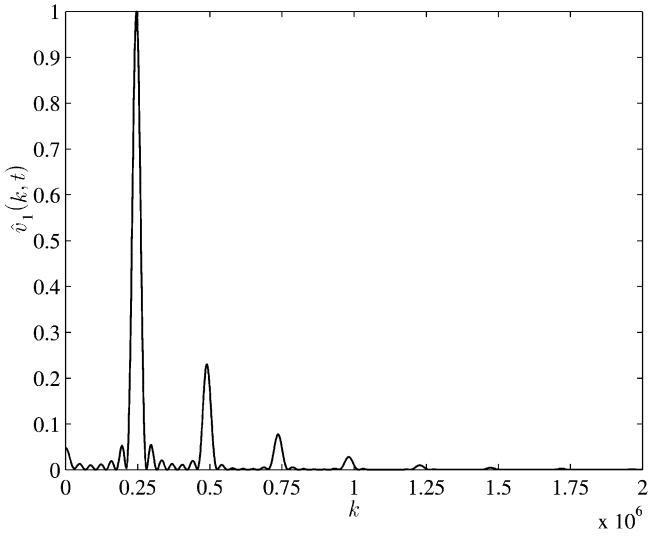

Fig. 9. Spatial FFT Eq. (30) of the particle velocity signal depicted in Fig. 6.

3.4. Double-wavenumber harmonic excitation

The results from the previous sections provide insight into the nonlinear dynamical behavior of pulses and waves in nonlinear media. Nevertheless, it is worthwhile examining the behavior of a double wavenumber sinusoidal (i.e. harmonic signals that contain two different wavenumbers) excitation in these nonlinear media. To this end, consider the initial value problem consisting of (20) with initial conditions

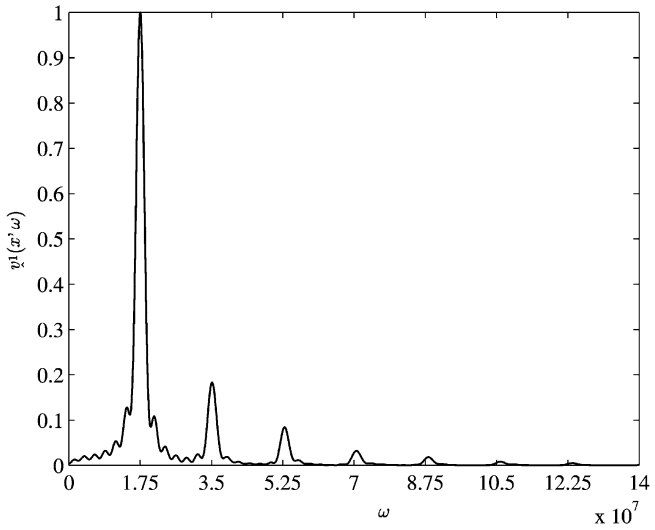

Fig. 10. Temporal FFT Eq. (31) of the particle velocity signal at $x = -150\Delta x$ depicted in Fig. 8.

$$u_{,x}(x, t = 0) = \begin{cases} A \sin k_1 x + B \sin k_2 x, & -150\Delta x \leqslant x \leqslant 150\Delta x, \\ 0, & \text{otherwise}, \end{cases} \tag{32}$$

$$u_{,t}(x, t = 0) = 0. \tag{33}$$

Numerical solutions to this initial value problem are carried out for $c = 70.71$ m/s, $\gamma = 10^4$ with $A = 4.9 \times 10^{-5}$, $B = 4.9 \times 10^{-5}$ and $k_1 = 3.0 \times 10^5$ m^{-1}, $k_2 = 5.0 \times 10^5$ m^{-1}. The initial excitation is shown in Fig. 11.

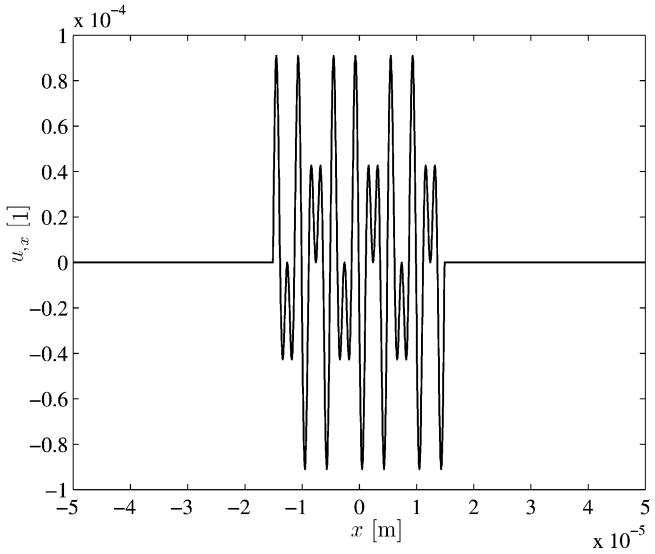

Fig. 11. Initial strain distribution $u_{,x}(x,t)$ given by Eq. (32).

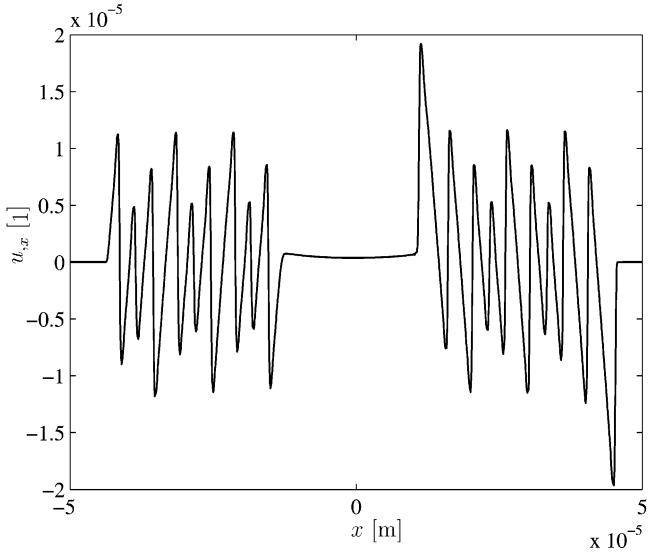

Fig. 12. Numerical solution for the strain wave at $t = 4.0 \times 10^{-7}$ s^{-2} wavenumbers.

The subsequent propagation of the disturbance is shown in Fig. 12 for $t = 4.0 \times 10^{-7}$ s. Similar results are shown in Fig. 13 for the particle velocity. It is seen from these Figures that, in a fashion similar to the single-frequency results in the previous section, there is a steepening of the wave front during propagation. The velocity profile resembles a sawtooth profile. This solution development is again based on the fact that different strain amplitudes propagate with different shift rates. As a result, the wave profiles broaden during unloading in compression ($u_{,x} < 0$) and loading in tension ($u_{,x} > 0$), while they steepen during unloading in tension and loading in compression. Because of the distortion, higher wavenumber components appear in

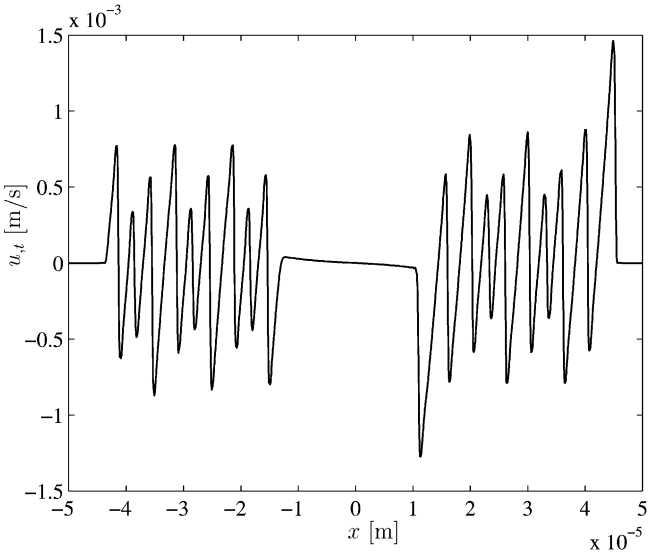

Fig. 13. Numerical solution for the particle velocity at $t = 4.0 \times 10^{-7}$ s^{-2} wavenumbers.

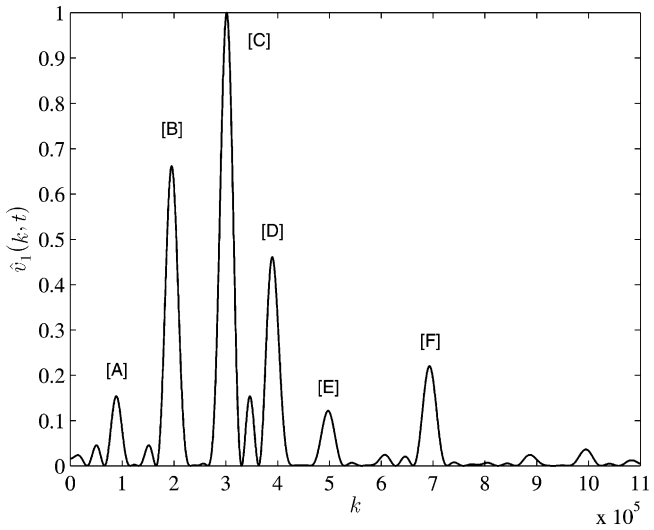

Fig. 14. Spatial FFT Eq. (30) for the particle velocity signal depicted in Fig. 13. Labels are explained in Table 1.

the propagating wave—for example, see Fig. 14 which shows the spatial FFT of the particle velocity at $t = 4.0 \times 10^{-7}$ s. However, unlike the case for the single-wavenumber harmonic excitation, the double wavenumber excitation yields not only multiples of the initial wavenumbers, but also combinations of the initial wavenumbers. The wavenumbers corresponding to some of the peaks in Fig. 14 are identified and explained in Table 1. If the medium is linear, the only peaks would be at $k = 3.0 \times 10^5$ m^{-1} and $k = 5.0 \times 10^5$ m^{-1}. Clearly, all other peaks (sum/difference combinations of the two primary wavenumbers) shown in Fig. 14 are due to the material nonlinearity.

When the nonlinearity is relatively week in comparison to the linear component (quasilinear), a perturbation method can be used to show (see e.g. Hamilton, 1998; Rudenko and Soluyan, 1977; Garett et al., 1983, 1984; Berntsen et al., 1984; Westervelt, 1963) that in a system with quadratic nonlinearity, the superposition of two progressive waves with distinctive wavenumbers (frequencies) will generate wavenumbers (frequencies) that are integer sum/difference combinations of the two primary frequencies, such as those observed in Table 1. For system with strong nonlinear effects and/or for compound waves, analytical solutions are no longer available. Therefore, it is unclear whether this is still true for strong nonlinear systems and for compound waves. However, the numerical results provided here seem to indicate that this phenomenon also occurs in systems with strong quadratic nonlinearity, and for compound waves as well.

Table 1
Sum/difference combinations of the two primary wavenumbers–quadratic nonlinearity

Position	Wavenumber ($k \times 10^5$)	Combination
$[A]$	1	$2k_1 - k_2$
$[B]$	2	$k_2 - k_1$
$[C]$	3	k_1
$[D]$	4	$2(k_2 - k_1)$
$[E]$	5	k_2
$[F]$	7	$2k_2 - k_1$

4. Wave propagation in hysteretic media—the Duhem model of active hysteresis

This section introduces the Duhem model for active hysteresis based on the considerations of Coleman and Hodgdon (1986), Hodgdon (1988a,b) and Macki et al. (1993). The Duhem model enables the description of active hysteresis by solutions to either a differential equation or an integral equation.

4.1. Theoretical concepts

The Duhem model focuses on the fact that the output of a hysteretic system can only change its character when the input changes direction. This model uses a phenomenological approach, postulating an integral operator or differential equation to model active hysteretic behavior. The work of Hodgdon (1988a,b), and Coleman and Hodgdon (1986) shows that such a model is useful in applied electromagnetics, because functions and parameters used in the model can be fine-tuned to match experimental results for a given situation. This research extends the Duhem model to mechanical waves in hysteretic media.

According to the Duhem model, the stress–strain relationship or the constitutive equation is governed by

$$\dot{\sigma} = \alpha \mid \dot{\epsilon} \mid (f(\epsilon) - \sigma) + \dot{\epsilon} g(\epsilon), \tag{34}$$

where σ denotes the stress and ϵ the strain. The material functions $f(\epsilon)$ and $g(\epsilon)$, as well as the parameter α obey certain restrictions. In order to study the solution character, divide (34) by $\dot{\epsilon} \neq 0$, which yields

$$\frac{\mathrm{d}\sigma}{\mathrm{d}\epsilon} = \alpha s(\dot{\epsilon})(f(\epsilon) - \sigma) + g(\epsilon), \tag{35}$$

where

$$s = \begin{cases} 1, & \text{for } \dot{\epsilon} > 0, \\ -1, & \text{for } \dot{\epsilon} < 0. \end{cases} \tag{36}$$

The resulting differential equation for $\dot{\epsilon} \neq 0$ can be solved for general functions of f and g

$$\sigma(\epsilon) = f(\epsilon) + (\sigma(\epsilon_0) - f(\epsilon_0))\mathrm{e}^{\alpha s(\epsilon_0 - \epsilon)} + \int_{\epsilon_0}^{\epsilon} (g(\tau) - f'(\tau))\mathrm{e}^{\alpha s(\tau - \epsilon)}\mathrm{d}\tau, \tag{37}$$

with ϵ_0 denoting the initial strain state. For the case $\dot{\epsilon} = 0$, Eq. (34) provides the solution

$$\sigma(\epsilon) = \sigma(\epsilon_0). \tag{38}$$

Hodgdon (1988b) proposes a sophisticated choice of the material functions f and g, i.e.

$$f = \begin{cases} A_1 \tan A_2 \epsilon, & \text{for } \mid \epsilon \mid \leqslant \epsilon^*, \\ A_1 \tan A_2 \epsilon^* + \frac{\epsilon - \epsilon^*}{\mu}, & \text{for } \epsilon > \epsilon^*, \\ -A_1 \tan A_2 \epsilon^* + \frac{\epsilon + \epsilon^*}{\mu}, & \text{for } \epsilon < -\epsilon^*, \end{cases} \tag{39}$$

and

$$g = \begin{cases} f'(\epsilon)\left[1 - A_3 \exp\left(\frac{A_4|\epsilon|}{\epsilon^* - |\epsilon|}\right)\right], & \text{for } \mid \epsilon \mid \leqslant \epsilon^* \\ f'(\epsilon), & \text{for } \mid \epsilon \mid > \epsilon^*. \end{cases} \tag{40}$$

The parameters $A_1[\mathrm{N/m^2}]$, $A_2[1]$, $A_3[1]$, $A_4[1]$, $\mu[\mathrm{m^2}/N]$ represent the degrees of freedom of this particular model needed to match experimental data or to obtain the desired hysteretic behavior by solving the system of equations consisting of (36)–(40). Due to its complexity, only a numerical treatment is considered, which is performed by Simpson's rule to approximate the solution to the integral equation (37).

In order to illustrate the character of this model, the solution to the combined equations for an exponentially decreasing harmonic input $\epsilon = 0.003\exp(-(t/5))\sin \pi t$ is shown in Fig. 15 for various parameter assignments. Note that the input and the parameters are chosen in this way only for the purpose of demonstrating the various emerging hysteretic effects. The hysteresis develops major and minor loops, and

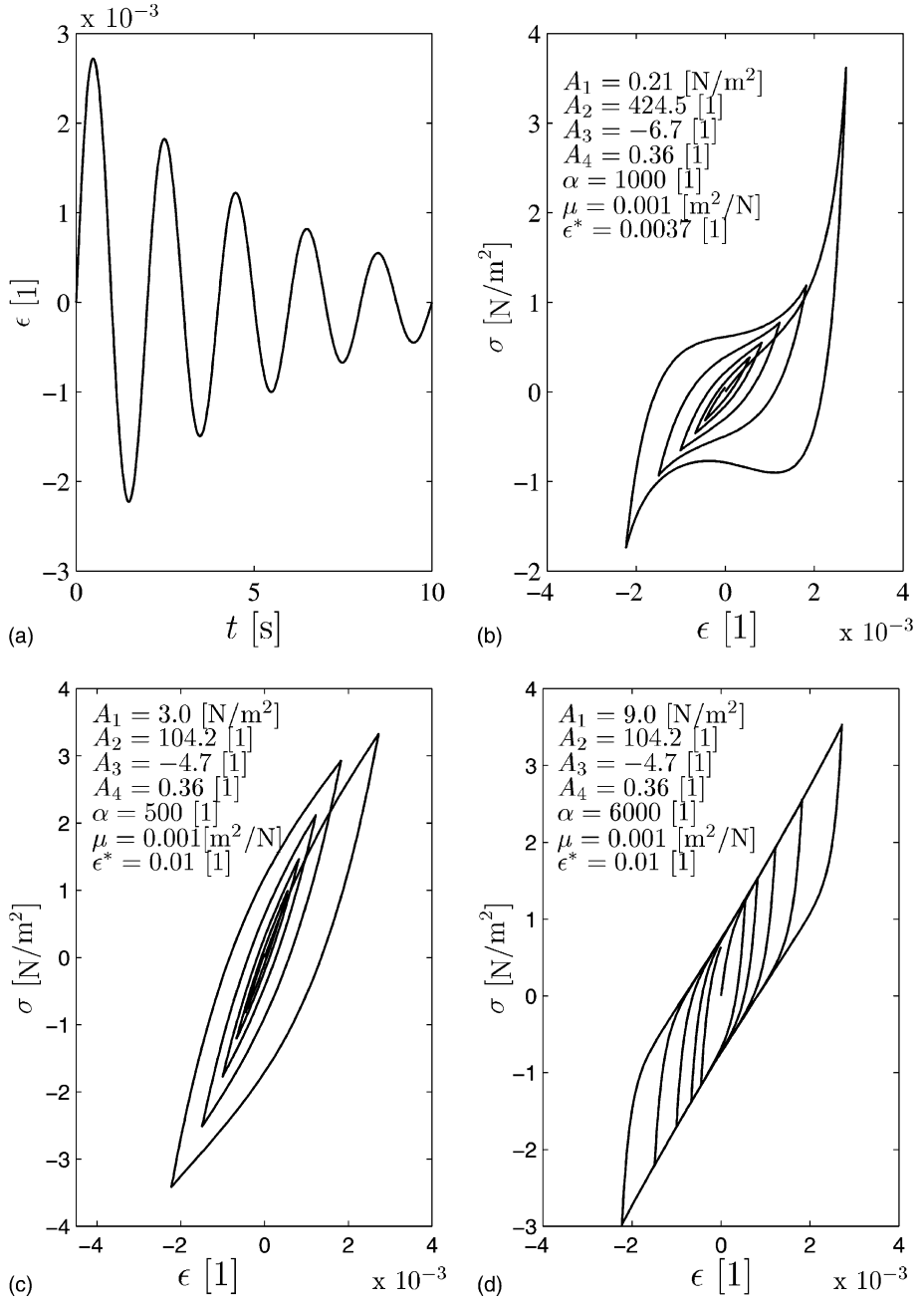

Fig. 15. System input $\epsilon(t)$ (a) and resulting hysteretic behavior for different parameter assignments (b)–(d).

hence the desired active hysteretic behavior. From a material point of view it can be deduced from Fig. 15 that for zero stress σ, the strain ϵ is not necessarily equal to zero, corresponding to residual strains and hence plastic deformation of the material. On the other hand, for zero strain ϵ, the corresponding stress σ is not necessarily equal to zero, corresponding to residual stresses. As a result, the proposed model allows for a general and combined treatment of various effects in hysteretic and/or plastically deformable materials.

The Hodgdon model for hysteresis (36)–(40) is used in the following sections to describe wave propagation (harmonic waves) in an active hysteretic media. If no further remarks are made, the Hodgdon hysteretic model is parameterized by the following assignments $A_1 = 50\,000$ N/m^2, $A_2 = 10.42$, $A_3 = -60.7$, $A_4 = 0.36$, $\alpha = 2.0 \times 10^6$, $\mu = 1.0$ m^2/N, and $\epsilon^* = 3.68$. It should be noted that these values are selected with some arbitrariness to illustrate the nonlinear effects. For practical applications, these parameters can be determined from experimental data.

The numerical solution algorithm is initialized with the following assignments: $\Delta x = 10^{-8}$ m, $\Delta t = 10^{-13}$ s to satisfy the CFL condition of the problem, and $\phi = 2.0$ for the least dissipative slope limiter.

4.2. Single-wavenumber harmonic excitation

Consider the excitation of this system with a single, harmonic signal at wave number k, applied as an initial condition for the strain $u_{,x}$ at time $t = 0$ for zero particle velocity $u_{,t}(x, t = 0)$, i.e.

$$u_{,x}(x, t = 0) = \begin{cases} A \sin kx, & \text{for } -100\Delta x \leqslant x \leqslant 100\Delta x \\ 0, & \text{otherwise,} \end{cases} \tag{41}$$

$$u_{,t}(x, t = 0) = 0 \tag{42}$$

with amplitude $A = 10^{-5}$ and wavenumber $k = 5.0 \times 10^6$ m^{-1} (Fig. 16). Numerical results for this type of excitation are shown in Figs. 17–27.

The results for the particle velocity (Fig. 17) and its spatial FFT (Fig. 18), respectively, show the development of higher harmonics, i.e. integer multiples of the initially applied wavenumber.

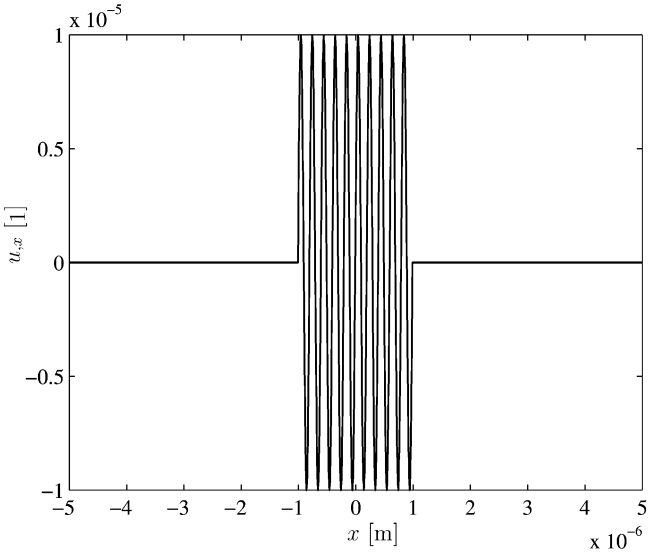

Fig. 16. Initial strain distribution $u_{,x}(x, t = 0)$ given by Eq. (41).

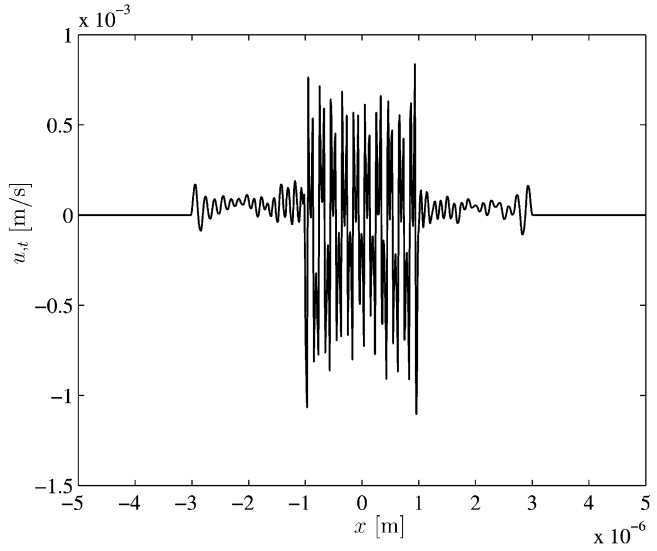

Fig. 17. Particle velocity $u_{,t}$ [m/s] vs. x at $t = 3.5 \times 10^{-10}$ s.

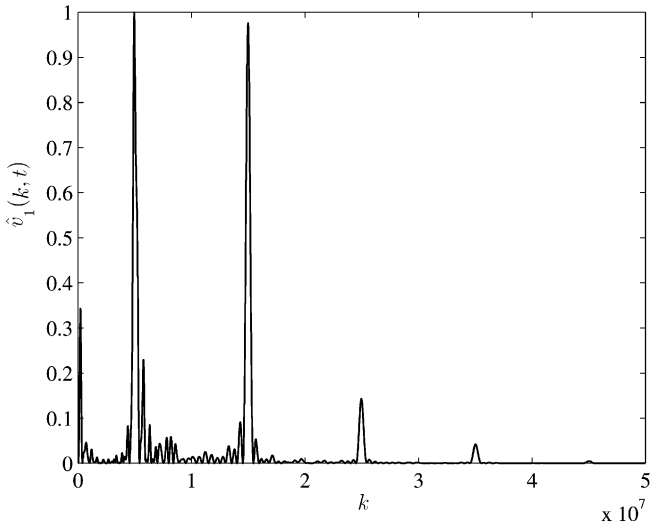

Fig. 18. Spatial FFT of the particle velocity signal in Fig. 17.

Compare these hysteretic effects with those obtained for the nonlinear elastic material considered in Section 3. Now, odd harmonics dominate the particle velocity signal. Such behavior was predicted, but not theoretically analyzed by Nazarov et al. (1988). This behavior means that a cubic or, generally, odd characteristic nonlinearity takes place, which is typical of metals with dislocations. Note, that this particular development is based on the fact that micro-plastic deformation takes place, as shown in Fig. 19. Here the numerical solution for the strain $u_{,x}$ is shown over the spatial coordinate x at time $t = 3.5 \times 10^{-10}$ s. There are only waves of very small amplitude emanating from the initially applied harmonic strain wave,

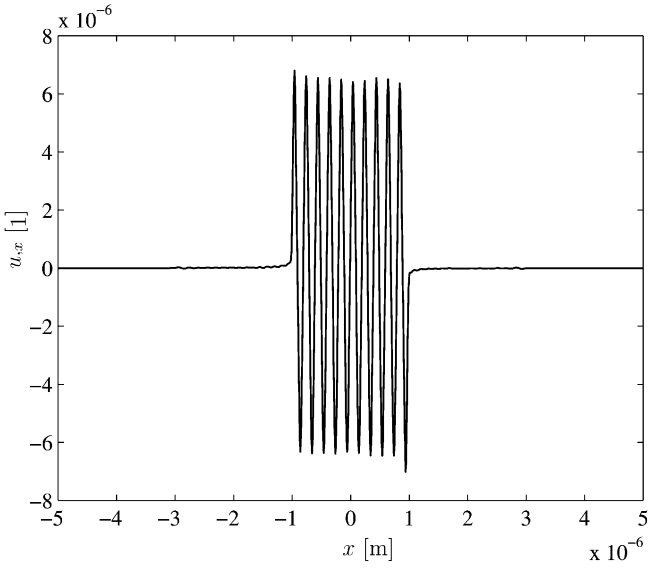

Fig. 19. Strain $u_{,x}$ vs. x at $t = 3.5 \times 10^{-10}$ s.

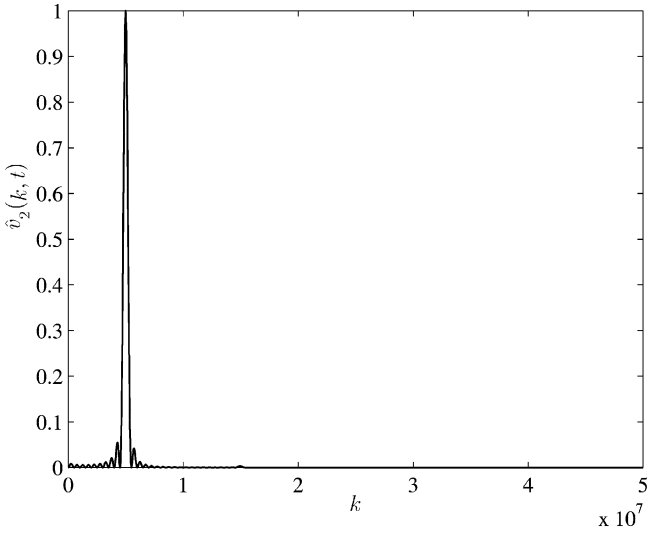

Fig. 20. Spatial FFT of the strain signal depicted in Fig. 19.

which still appears at the initial location, in addition to some small distortions. Note, that no higher harmonics or wavenumber changes appear in the strain signal over space (Fig. 20).

Consider now the hysteretic stress–strain relation as illustrated in Fig. 21, where the stress is plotted over strain at the spatial point $x = -110\Delta x$ with time t as the parameter. The development of residual strains is obvious—the stress oscillates around the zero stress state with decreasing amplitude, while the strain tends to a nonzero value.

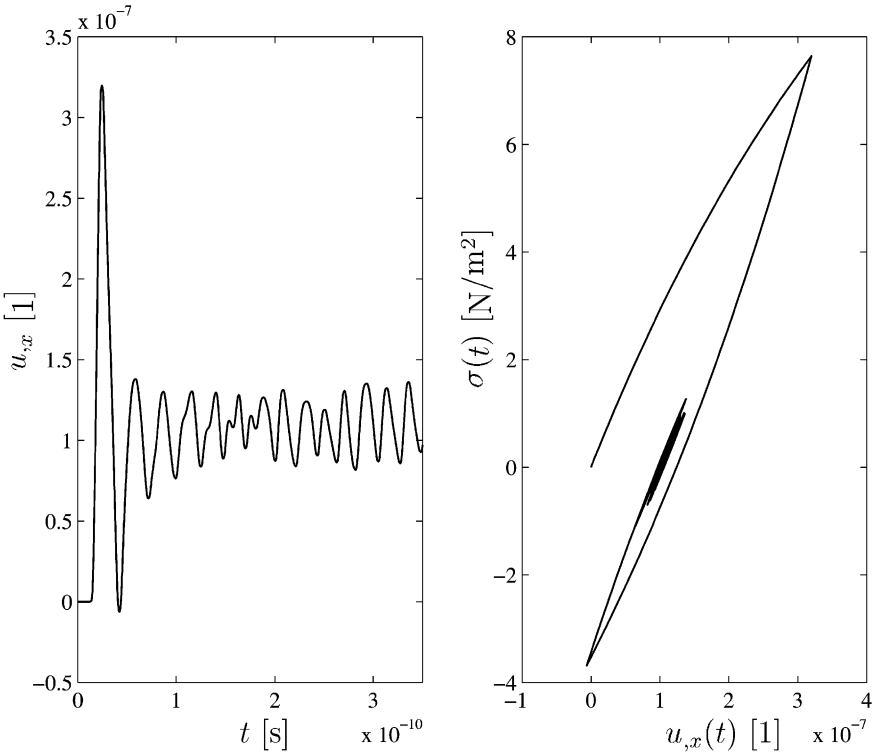

Fig. 21. Strain (left) and corresponding stress–strain relation (right) at $x = -110\Delta x$.

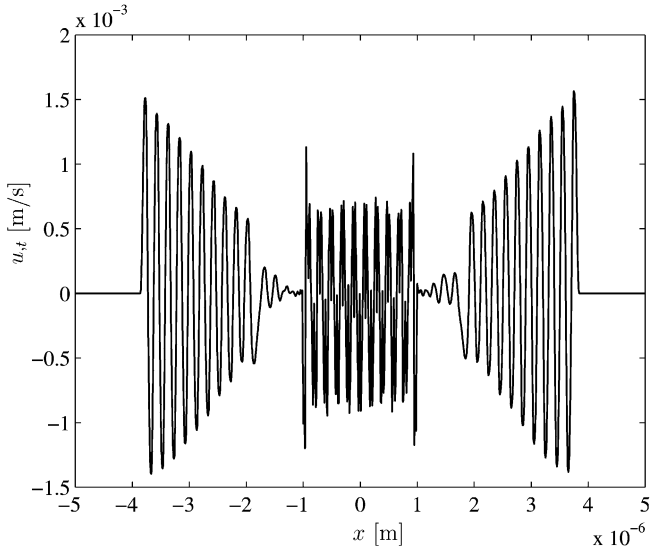

Fig. 22. Particle velocity $u_{,t}$ [m/s] vs. x at $t = 3.5 \times 10^{-10}$ s for $\alpha = 2.0 \times 10^5$.

This solution behavior can be explained using the development of residual strains, which correspond to micro-plastic deformation. The values that describe the hysteretic loops are chosen in such a way that the

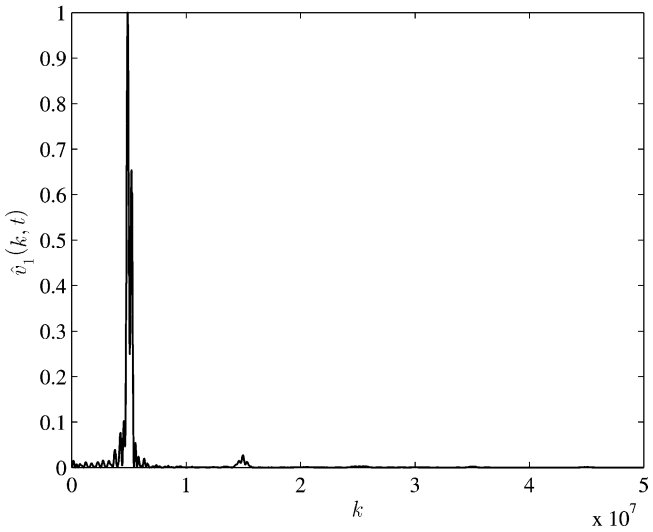

Fig. 23. Spatial FFT of the particle velocity signal in Fig. 22.

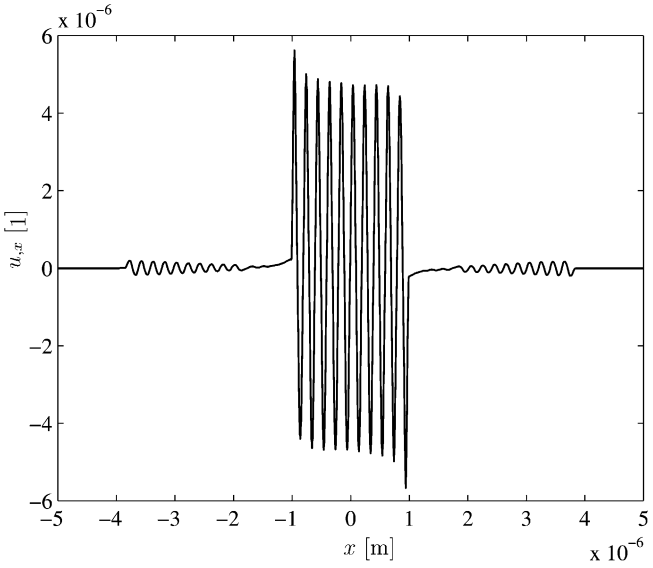

Fig. 24. Strain $u_{,x}$ vs. x at $t = 3.5 \times 10^{-10}$ s for $\alpha = 2.0 \times 10^5$.

plastic deformation prevents almost all wave propagation. This is the case because the energy that is initially fed into the system by the harmonic strain wave of Fig. 16 is consumed by plastic deformation of the media. As a result, there is not enough energy left to develop a propagating strain wave. In order to illustrate this fact, numerical experiments are performed by changing the hysteretic parameter α from 2.0×10^6 to 2.0×10^5, corresponding to a change of the hysteresis shape and amplitude. These results are shown in Figs. 22–26.

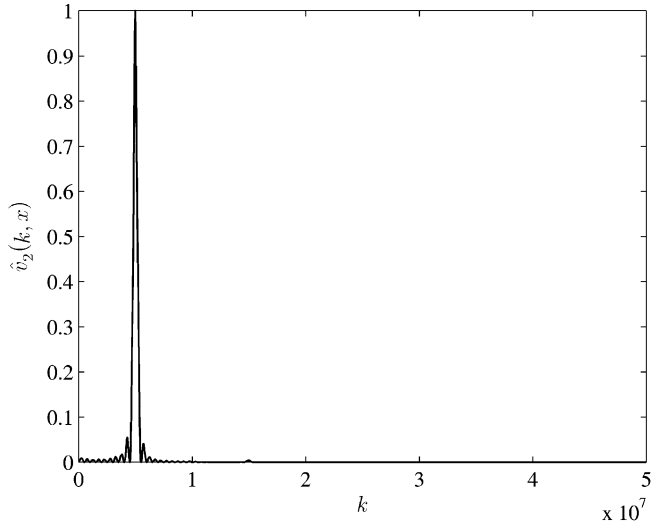

Fig. 25. Spatial FFT of the strain signal depicted in Fig. 24.

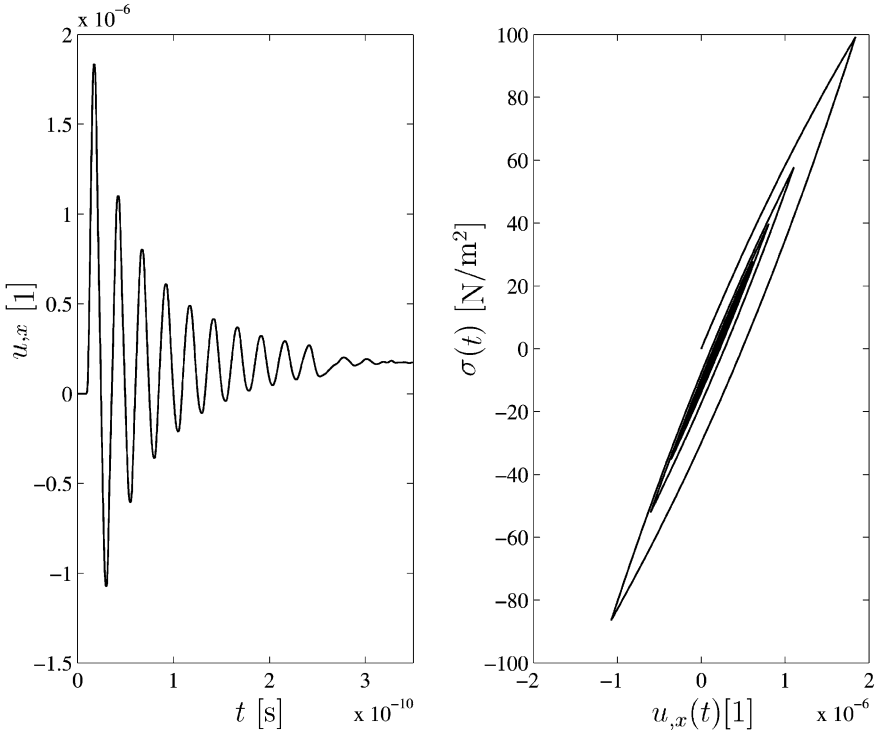

Fig. 26. Strain (left) and corresponding stress–strain relation (right) at $x = -110\Delta x$ for $\alpha = 2.0 \times 10^5$.

It is obvious that the solution behavior differs significantly from the solution obtained with the larger value of α. There are harmonic particle velocity waves propagating to the left ($x \downarrow$) and to the right ($x \uparrow$),

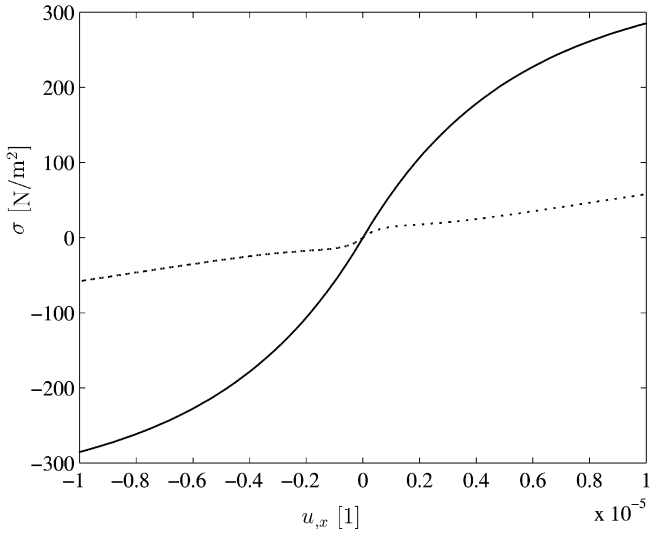

Fig. 27. Comparison of the strain energy input by initial condition Eq. (41) for $\alpha = 2.0 \times 10^6$ (solid) and $\alpha = 2.0 \times 10^5$ (dotted).

while odd harmonics still appear in the signal (Figs. 22 and 23)—recall that the initial particle velocity is assigned a value of zero, $u_{,t}(x, t = 0) \equiv 0$. Furthermore, strain waves emanate from the initial profile, which remains similar to its initial shape and position, except with a smaller amplitude (Figs. 24 and 25). Compared to the results for the same system, but with $\alpha = 2.0 \times 10^6$ (shown in Fig. 19), there are clearly strain waves evolving and propagating. In order to illustrate the hysteretic system behavior, the numerical solution at $x = -110\Delta x$ for strain vs. time and stress vs. strain, respectively is shown in Fig. 26. Note that the amplitude of the stress developed is decisively larger than the one for the same system with $\alpha = 2.0 \times 10^6$. On the other hand, the system still develops residual strains corresponding to micro-plastic deformation. Summarizing these results, one can conclude, that the energy put into this particular system with $\alpha = 2.0 \times 10^5$ is not completely consumed by the plastic deformation of the media, and hence the evolution of the harmonic particle velocity and strain waves can be observed. This explanation is confirmed by considering the amount of strain energy put into the two hysteretic systems by the initially applied harmonic strain wave. In Fig. 27 the stress–strain relation for one spatial sinusoidal strain cycle is shown for $\alpha = 2.0 \times 10^5$ (solid) and $\alpha = 2.0 \times 10^6$ (dotted). The strain energy put into a particular system is given by the area under each curve, multiplied by the number of applied cycles—note, spatial behavior is considered, and as a result the absolute values of the area under the positive and negative parts of the curves have to be summed. One can easily verify that the energy input into the system with $\alpha = 2.0 \times 10^5$ is much larger than the input into the system with $\alpha = 2.0 \times 10^6$, respectively. Based on this fact, and the energy consumed by traversing the hysteresis, the reason for the lack of existence of harmonic waves in the case of a larger value of the hysteretic parameter α becomes apparent.

4.3. Double-wavenumber harmonic excitation

The results obtained for the double-wavenumber harmonic strain excitation of a quadratic nonlinear media (Section 3) clearly provide a tool to determine the nonlinearity of a given system. Consider now the excitation of the Hodgdon model (36)–(40) by a harmonic strain wave applied as an initial condition and containing two wavenumbers k_1, k_2, i.e.

$$u_{,x}(x,t=0)=\begin{cases} A\sin k_1 x + B\sin k_2 x, & \text{for } -100\Delta x \leqslant x \leqslant 100\Delta x,\\ 0, & \text{otherwise.}\end{cases} \tag{43}$$

$$u_{,t}(x,t=0)=0. \tag{44}$$

The parameters A and B denote the amplitudes of each sinusoidal wave. If no further remarks are made, the following values for the excitation are assigned: $A = 5.0\times10^{-6}$, $B = 5.0\times10^{-6}$, $k_1 = 12.0\times10^{6}$ m^{-1}, and $k_2 = 15.0\times10^{6}$ m^{-1}. The emerging waves are shown and analyzed in Figs. 28–30. The hysteretic model is parameterized by $A_1 = 50\,000$, $A_2 = 10.42$, $A_3 = -60.7$, $A_4 = 0.36$, $\alpha = 2.0\times10^{6}$, $v = 1.0$, and $\epsilon^* = 3.68$.

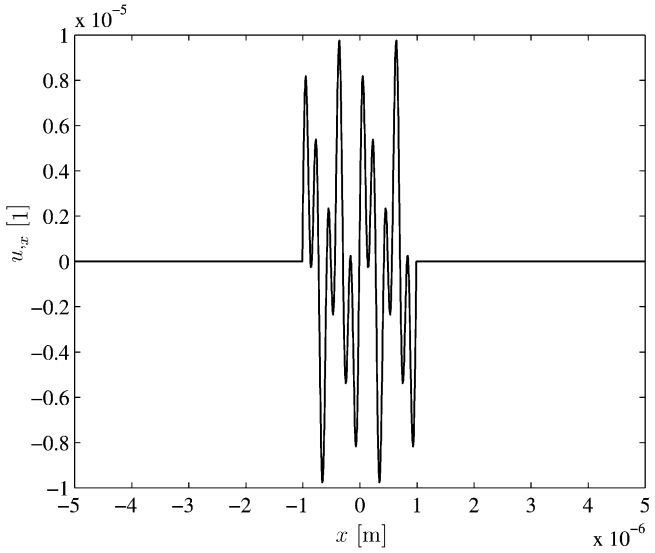

Fig. 28. Initial strain distribution $u_{,x}(x,0)$ given by Eq. (43).

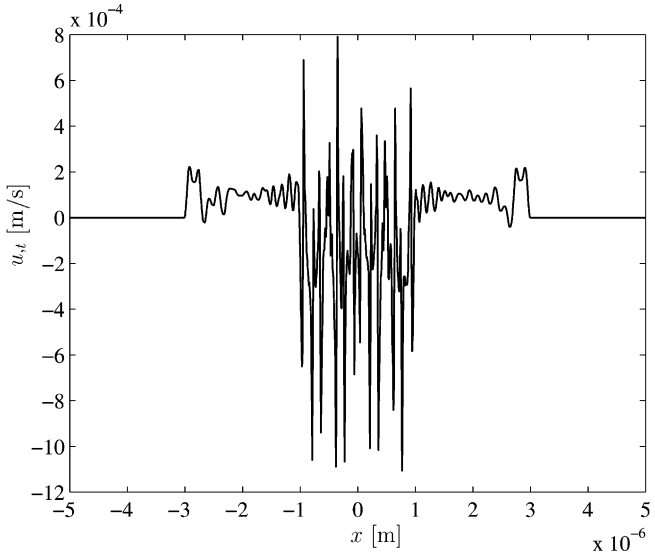

Fig. 29. Numerical solution for the particle velocity at $t = 3.5\times10^{-10}$ s^{-2} wavenumbers.

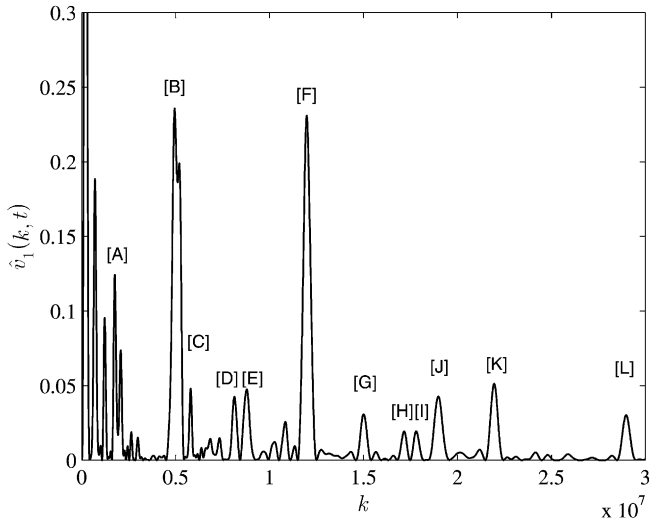

Fig. 30. Spatial FFT Eq. (30) of the particle velocity signal depicted in Fig. 29. Labels are explained in Table 2.

Table 2
Sum/difference combinations of the two primary wavenumbers–hysteresis

Position	Wavenumber $k \times 10^6$	Combination
$[A]$	2.0	k_1
$[B]$	5.0	k_2
$[C]$	6.0	$3k_1$
$[D]$	8.0	$2k_2 - k_1$
$[E]$	9.0	$k_2 + 2k_1$
$[F]$	12.0	$2k_2 + k_1$
$[G]$	15.0	$3k_2$
$[H]$	17.0	$3k_2 + k_1$
$[I]$	18.0	$4k_2 - k_1$
$[J]$	19.0	$3k_2 + 2k_1$
$[K]$	22.0	$4k_2 + k_1$
$[L]$	29.0	$5k_2 + 2k_1$

Fig. 28 shows the initial strain distribution. The numerical solution for the particle velocity and an enlarged plot of its spatial FFT (30) at time $t = 3.5 \times 10^{-10}$ s are shown in Figs. 29 and 30. The characteristic appearance of odd harmonics in the single-wavenumber case, here corresponding to $3k_1$ and $3k_2$, are confirmed using the results in Fig. 30. Besides odd harmonics, the signal contains combinations of the excitation wavenumbers as summarized in Table 2. Again, the appearance of wavenumber combinations can be clearly determined as a nonlinear effect in media governed by history- and non history-dependent constitutive equations.

5. Summary and conclusion

This paper presents a second-order, high-resolution central scheme that is used to develop a computer program for the solution of problems of wave propagation in nonlinear and hysteretic media. The effec-

tiveness and robustness of the computer program is demonstrated by analyzing wave propagation in several nonlinear and hysteretic media. The numerical solver provides a high resolution of the nonlinear effects that evolve during wave propagation, such as the development of shock and rarefaction waves. Furthermore, since the solver implemented in this study is independent of the eigenstructure of the system under consideration, it can be used for a broad class of quasilinear systems of conservation laws and convection diffusion equations.

The constitutive law used in this paper is based on the Duhem model of hysteresis. The corresponding stress–strain relationship is in terms of an integral form. It is shown that this stress–strain relationship is rather general in that several well-known constitutive laws studies in the literature are its special cases.

Numerical results show that a wave of a single wavenumber propagating in nonlinear elastic media generates both even and odd harmonics, while the same wave propagating in hysteretic media generates mostly odd harmonics. The excitation of hysteretic and nonhysteretic media by harmonic signals containing two different fundamental wavenumbers is also studied. The results clearly show the generation of wavenumber combinations, or sidebands. Note that this is not the case for a purely linear-elastic media, making these higher harmonics an ideal candidate metric to characterize nonlinear media. It is interesting to note that the appearance of wavenumber combinations is most intense for the case of hysteretic media.

Finally, it is important to note that hysteresis consumes a portion of the input energy. This consumption (loss) of energy makes a hysteretic medium distinctly different from a nonlinear elastic medium—the numerical results confirm this behavior.

Appendix A. Analytical solution to the Riemann problem for the quadratic nonlinearity

The considered quasi-linear hyperbolic two-system of conservation laws, i.e.

$$\frac{\partial}{\partial t}\begin{bmatrix} v_1 \\ v_2 \end{bmatrix} + \frac{\partial}{\partial x}\begin{bmatrix} -c^2 v_2\left(1-\frac{\gamma}{2}v_2\right) \\ -v_1 \end{bmatrix} = 0, \tag{A.1}$$

with phase velocity $c = \sqrt{E/\rho}$ allows the derivation of an analytical solution if discontinuous initial conditions

$$\mathbf{v}(x, t=0) = \begin{cases} \mathbf{v}_{\mathrm{L}} & \text{for } x < 0, \\ \mathbf{v}_{\mathrm{R}} & \text{for } x > 0. \end{cases} \tag{A.2}$$

are prescribed. In the following, the results obtained are summarized based on the considerations in Meurer (2000). The pursued analysis shows that the solution to the considered quasi-linear Riemann problem consists of two rarefaction curves and two shock curves in state space (v_1, v_2), which connect the states on the left and right of the initial discontinuity. Hence, the following equations hold for the one-rarefaction curve $\left(v_{2_{\mathrm{L}}} \leqslant v_2 < \left(\frac{1}{\gamma}\right)\right)$

$$R_1(\mathbf{v}, \mathbf{v}_{\mathrm{L}}) = v_1 - v_{1_{\mathrm{L}}} + \frac{2c}{3\gamma}\left(\sqrt{(1-\gamma v_2)^3} - \sqrt{(1-\gamma v_{2_{\mathrm{L}}})^3}\right) = 0, \tag{A.3}$$

the two-rarefaction curve $\left(v_{2_{\mathrm{R}}} \leqslant v_2 < \frac{1}{\gamma}\right)$

$$R_2(\mathbf{v}, \mathbf{v}_{\mathrm{R}}) = v_{1_{\mathrm{R}}} - v_1 - \frac{2c}{3\gamma}\left(\sqrt{(1-\gamma v_{2_{\mathrm{R}}})^3} - \sqrt{(1-\gamma v_2)^3}\right) = 0, \tag{A.4}$$

the one-shock curve $\left(v_2 \leqslant v_{2_{\mathrm{L}}} < \frac{1}{\gamma}\right)$

$$S_1(\mathbf{v}, \mathbf{v}_{\mathrm{L}}) = v_1 - v_{1_{\mathrm{L}}} + c(v_{2_{\mathrm{L}}} - v_2)\sqrt{1 - 0.5\gamma(v_2 + v_{2_{\mathrm{L}}})} = 0, \tag{A.5}$$

and the two-shock curve $\left(v_2 \leqslant v_{2_R} < \frac{1}{\gamma}\right)$

$$S_2(\mathbf{v}, \mathbf{v}_R) = v_{1_R} - v_1 + c(v_{2_R} - v_2)\sqrt{1 - 0.5\gamma(v_2 + v_{2_R})} = 0. \tag{A.6}$$

The states $\mathbf{v}_L$ and $\mathbf{v}_R$ are connected by an intermediate state or connecting state, respectively, which itself depends on the prescribed values of the initial conditions (A.2). Consider the case of a connection one-shock, two-rarefaction. Then the following algebraic equations have to be solved, yielding the evolving intermediate state $\bar{\mathbf{v}}$

$$\left.\begin{array}{l} S_1(\bar{\mathbf{v}}, \mathbf{v}_L) = 0 \\ R_2(\bar{\mathbf{v}}, \mathbf{v}_R) = 0 \end{array}\right\} \Rightarrow \bar{\mathbf{v}}. \tag{A.7}$$

The rarefaction waves represent self-similar solutions, i.e. solutions of the form

$$\mathbf{v}(x, t) = \mathbf{w}(\xi = x/t). \tag{A.8}$$

They can be determined by a normalization process (Godlewski and Raviart, 1996), providing the following expressions (Meurer, 2000) in terms of ξ for the one-rarefaction wave

$$w_1^{(1)} = v_{1_L} - \frac{2c}{3\gamma}\left(\sqrt{(1 - \gamma w_2^{(1)})^3} - \sqrt{(1 - \gamma v_{2_L})^3}\right), \tag{A.9}$$

$$w_2^{(1)} = \frac{1}{\gamma}\left(1 - \left(\sqrt{1 - \gamma v_{2_L}} - \frac{\xi - v_1(v_{2_L})}{c}\right)^2\right), \tag{A.10}$$

and similarly for the two-rarefaction wave

$$w_1^{(2)} = \bar{v}_1 + \frac{2c}{3\gamma}\left(\sqrt{(1 - \gamma w_2^{(2)})^3} - \sqrt{(1 - \gamma \bar{v}_2)^3}\right), \tag{A.11}$$

$$w_2^{(2)} = \frac{1}{\gamma}\left(1 - \left(\sqrt{1 - \gamma \bar{v}_2} + \frac{\xi - v_2(\bar{v}_2)}{c}\right)^2\right), \tag{A.12}$$

with $\bar{\mathbf{v}}$ denoting the evolving intermediate state.

In order to determine the shock waves, recall that along any line of discontinuity a weak solution of $\mathbf{v}$ of

$$\frac{\partial \mathbf{v}}{\partial t} + \frac{\partial \mathbf{f}}{\partial x} = \mathbf{0}, \tag{A.13}$$

satisfies the Rankine–Hugoniot condition (Godlewski and Raviart, 1996; Thomas, 1999). This allows together with the Lax entropy condition (Godlewski and Raviart, 1996; Thomas, 1999) the determination of the admissible shock curves (A.5) and (A.6) and hence the shock speeds for the one- and two-shock wave

$$s^{(1)} = -c\sqrt{1 - 0.5\gamma(\bar{v}_2 + v_{2_L})}, \tag{A.14}$$

$$s^{(2)} = c\sqrt{1 - 0.5\gamma(\bar{v}_2 + v_{2_R})}. \tag{A.15}$$

Appendix B. Numerical solution algorithm

In order to approximate the solution to the considered problem of wave propagation in nonlinear hysteretic media, a second-order central scheme proposed by Kurganov and Tadmor (2000) was imple-

mented, providing high-resolution of any nonlinear effect while retaining the simplicity of a Riemann solver free approach. It can be directly applied to equations in conservation form as (16) and allows extensions to multidimensional systems of conservation laws and convection–diffusion equations with and without source terms. Furthermore, it allows a semi-discrete formulation (method of lines) which has to be coupled with appropriate ODE-solvers. The main idea of the scheme (in brief) is to include more precise information about the local speed of wave propagation, in order to average the nonsmooth parts of the computed solution over smaller cells of variable size of order $\mathcal{O}(\Delta t)$. Besides being independent of the eigenstructure of the problem under consideration, the modern representatives of central schemes enjoy a much smaller numerical viscosity than their forerunners, e.g. the Lax–Friedrichs scheme. In the present case, the numerical viscosity of the Kurganov–Tadmor scheme is proportional to $\mathcal{O}(\Delta x^{2r-1})$, $r \in \mathcal{N}$ whereby many central schemes share excessive numerical viscosity of order $\mathcal{O}(\Delta x^{2r}/\Delta t)$, $r \in \mathcal{N}$, smearing out any nonlinear effects. This fact become apparent since numerical stability and the CFL condition generally speaking require $\Delta t \ll \Delta x$. As a result the numerical viscosity might dominate the resolution capabilities of the numerical algorithm.

The fully-discrete version of the scheme for the case of one-dimensional conservation laws (16) is summarized below. Let $\mathbf{v}(x_j, t_n) = \mathbf{u}_j^n$, then the algorithm is given by

$$\mathbf{u}_j^{n+1} = \lambda a_{j-\frac{1}{2}}^n \mathbf{w}_{j-\frac{1}{2}}^{n+1} + \left[1 - \lambda(a_{j-\frac{1}{2}}^n + a_{j+\frac{1}{2}}^n)\right]\mathbf{w}_j^{n+1} + \lambda a_{j+\frac{1}{2}}^n \mathbf{w}_{j+\frac{1}{2}}^{n+1} + \frac{\Delta x}{2}\left[(\lambda a_{j-\frac{1}{2}}^n)^2 (\mathbf{u}_{,x})_{j-\frac{1}{2}}^{n+1} - (\lambda a_{j+\frac{1}{2}}^n)^2 (\mathbf{u}_{,x})_{j+\frac{1}{2}}^{n+1}\right], \tag{B.1}$$

with the reconstructed slopes $(\mathbf{u}_{,x})_{j-(1/2)}^{n+1}$, the intermediate values $\mathbf{w}_j^{n+1}$, and the local speed of propagation $a_{j+(1/2)}^n$. Minmod and minmod-like limiters are used to reconstruct the appearing derivatives with respect to x. For further details consult Kurganov and Tadmor (2000). The ratio $\lambda = (\Delta t/\Delta x)$, with Δt the temporal step and Δx the spatial step, has to be chosen appropriately in order to satisfy the CFL condition which can be considered as a necessary condition for convergence of nonlinear difference schemes (see e.g. Godlewski and Raviart, 1996).

References

Achenbach, J.D., 1999. Wave Propagation in Elastic Solids. Elsevier Science Publishers BV, Amsterdam.

Berntsen, J., Tjøtta, J.N., Tjøtta, S., 1984. Nearfield of a large acoustic transducer, Part IV: Second harmonic and sum frequency radiation. Journal of the Acoustical Society of America 75, 1383–1391.

Bland, D.R., 1969. Nonlinear Dynamic Elasticity. Blaisdell Publishing Company, Waltham, Massachusetts.

Cantrell, J.H., Yost, W.T., 1990. Material characterization using acoustic nonlinearity parameters and harmonic generation: effects of crystalline and amorphous structures. Review of Progress in QNDE 13B, 1661–1668.

Coleman, B.D., Hodgdon, M.L., 1986. On a class of constitutive relations for ferromagnetic hysteresis. International Journal of Engineering Science 24 (6), 897–919.

Courant, R., Friedrichs, K.O., 1976. Supersonic Flow and Shock waves. Applied Mathematical Sciences, vol. 2. Springer, Berlin.

Debnath, L., 1997. Nonlinear Partial Differential Equations for Scientists and Engineers. Birkhauser..

Drumheller, D.S., 1998. Introduction to Wave Propagation in Nonlinear Fluids and Solids. Cambridge University Press, Cambridge.

Garett, G.S., Tjøtta, J.N., Tjøtta, S., 1983. Nearfield of a large acoustic transducer, Part II: Parametric radiation. Journal of the Acoustical Society of America 74, 1013–1020.

Garett, G.S., Tjøtta, J.N., Tjøtta, S., 1984. Nearfield of a large acoustic transducer. Part III: General results. Journal of the Acoustical Society of America 75, 769–779.

Godlewski, E., Raviart, P.A., 1996. Numerical Approximation of Hyperbolic Systems of Conservation Laws. Applied Mathematical Sciences,vol. 118. Springer-Verlag, New York/Berlin.

Gol'dberg, Z.A., 1961. Interaction of plane longitudinal and transverse elastic waves. Soviet Physics, Acoustics 6, 306–310.

Guyer, R.A., McCall, K.R., 1995. Hysteresis, discrete memory, and nonlinear wave propagation in rock: a new paradigm. Physical Review Letters 74 (17), 3491–3494.

Gusev, V., 2000. Propagation of acoustic pulses in material with hysteretic nonlinearity. Journal of the Acoustical Society of America 107 (6), 3047–3058.
Hamilton, M.F., Blackstock, D.T. (Eds.), 1998. Nonlinear Acoustics. Academic Press, San Diego.
Hamilton, M.F., 1998. Sound beams. In: Hamilton, M.F., Blackstock, D.T. (Eds.), Nonlinear Acoustics, Chapter 8. Academic Press, San Diego.
Hodgdon, M.L., 1988a. Application of a Theory of Ferromagnetic Hysteresis. IEEE Transactions on Magnetics 24 (1), 218–221.
Hodgdon, M.L., 1988b. Mathematical Theory and Calculations of Magnetic Hysteresis Curves. IEEE Transactions on Magnetics 24 (6), 3120–3122.
Kolsky, H., 1963. Stress Waves in Solids. Dover Publications, New York.
Kurganov, A., Tadmor, E., 2000. New high-resolution central schemes for nonlinear conservation laws and convection–diffusion equations. Journal of Computational Physics 160, 241–282.
Landau, L.D., Lifshitz, E.M., 1959. Theory of Elasticity. Pergamon Press, New York.
Liu, G., Qu, J., Jacobs, L.J., 2000. Effects of cure state on the ultrasonic nonlinear parameter in adhesive joints. ASME AMD 240, 83–94.
Macki, J.W., Nistri, P., Zecca, P., 1993. Mathematical models for hysteresis. SIAM Review 35 (1), 94–123.
Mayergoyz, I.D., 1991. Mathematical Models of Hysteresis. Springer, Berlin.
McCall, K.R., 1994. Theoretical study of nonlinear elastic wave propagation. Journal of Geophysical Research 99 (B2), 2591–2600.
McCall, K.R., Guyer, R.A., 1994. Equation of state and wave propagation in hysteretic nonlinear elastic materials. Journal of Geophysical Research 99 (B12), 23887–23897.
McCall, K.R., Guyer, R.A., 1996. A New theoretical paradigm to describe hysteresis, discrete memory and nonlinear elastic wave propagation in rock. Nonlinear Processes in Geophysics 3, 89–101.
Meurer, T., 2000. Wave Propagation in Hysteretic Media. MS. Thesis, School of Civil and Environmental Engineering, Georgia Institute of Technology, Atlanta.
Naugolnykh, K., Ostrovsky, L., 1998. Nonlinear wave processes in acoustics. Cambridge Texts in Applied Mathematics. Cambridge University Press, Cambridge.
Nazarov, V.E., Ostrovsky, L., Soustova, I.A., Sutin, A.M., 1988. Nonlinear acoustics of micro-inhomogeneous media. Physics of Earth and Planetary Interiors 50, 65–73.
Norris, A.N., 1998. Finite-amplitude waves in solids. In: Hamilton, M.F., Blackstock, D.T. (Eds.), Nonlinear Acoustics, Chapter 9. Academic Press, San Diego.
Rudenko, O.V., Soluyan, S.I., 1977. Theoretical Foundations of Nonlinear Acoustics. Plenum Publishing, New York.
Taylor, M.E., 1996. Partial Differential Equations III-Nonlinear Equations. Applied Mathematical Sciences, vol. 117. Springer, Berlin.
Thomas, J.W., 1995. Numerical Partial Differential Equations—Finite Difference Methods. Texts in Applied Mathematics, vol. 22. Springer, Berlin.
Thomas, J.W., 1999. Numerical Partial Differential Equations—Conservation Laws and Elliptic Equations. Texts in Applied Mathematics, vol. 33. Springer, Berlin.
Abeele, K.E.-A., Johnson, P.A., Sutin, A., 2000a. Nonlinear elastic wave spectroscopy (NEWS) techniques to discern material damage, Part I: Nonlinear wave modulation spectroscopy (NWMS). Research in Non-Destructive Evaluation 12 (1), 17–30.
Abeele, K.E.-A., Carmeliet, J., Cate, J.A., Johnson, P.A., 2000b. Nonlinear elastic wave spectroscopy (NEWS) techniques to discern material damage, Part II: Single-mode nonlinear resonance acoustic spectroscopy. Research in Non-Destructive Evaluation 12 (1), 31–42.
Wendroff, B., 1972a. The Riemann problem for materials with nonconvex equations of state. I: Isentropic flow. Journal of Mathematical Analysis and Applications 38, 454–466.
Wendroff, B., 1972b. The Riemann problem for materials with nonconvex equations of state. II: General flow. Journal of Mathematical Analysis and Applications 38, 640–658.
Westervelt, P.J., 1963. Parametric Acoustic Array. Journal of the Acoustical Society of America 35, 535–537.
Whitham, G.B., 1999. Linear and Nonlinear Waves. Pure and Applied Mathematics, vol. 1237. Wiley, New York.